PHYSICAL REVIEW A **95**, 062338 (2017)

Quantum error-correction failure distributions: Comparison of coherent and stochastic error models

Jeff P. Barnes,[1,*] Colin J. Trout,[1,2] Dennis Lucarelli,[1] and B. D. Clader[1]
[1]*Johns Hopkins University Applied Physics Laboratory 11100 Johns Hopkins Road, Laurel, Maryland 20723, USA*
[2]*School of Chemistry and Biochemistry, Georgia Institute of Technology, Atlanta, Georgia 30332, USA*

(Received 12 April 2017; published 29 June 2017)

We compare failure distributions of quantum error correction circuits for stochastic errors and coherent errors. We utilize a fully coherent simulation of a fault-tolerant quantum error correcting circuit for a $d = 3$ Steane and surface code. We find that the output distributions are markedly different for the two error models, showing that no simple mapping between the two error models exists. Coherent errors create very broad and heavy-tailed failure distributions. This suggests that they are susceptible to outlier events and that mean statistics, such as pseudothreshold estimates, may not provide the key figure of merit. This provides further statistical insight into why coherent errors can be so harmful for quantum error correction. These output probability distributions may also provide a useful metric that can be utilized when optimizing quantum error correcting codes and decoding procedures for purely coherent errors.

DOI: 10.1103/PhysRevA.95.062338

I. INTRODUCTION

The theory of fault tolerance and the associated threshold theorem show that given an error rate on physical qubits below some threshold, one can perform a quantum computation with arbitrary accuracy with manageable overhead due to error correction (see e.g., Refs. [1–9]). It is well known that the Pauli matrices form a basis for any arbitrary qubit state. Therefore any arbitrary unitary evolution can be written as a linear combination of Pauli matrices. Thus, it is sufficient to correct only for these types of errors in quantum error correction [10].

This fact often leads to a logical leap that is not always justified. In particular, in numerical simulations of quantum error correction routines, it is standard practice to only consider stochastic Pauli errors. In some cases such a model is valid. For example, in models of open quantum systems [11–13], the system environment coupling causes the environment to constantly "measure" the qubits. This can cause qubit depolarization, which can be modeled as the mapping of the qubit density matrix

$$\rho \to (1 - p_1 - p_2 - p_3)\rho + p_1\mathbf{X}\rho\mathbf{X} + p_2\mathbf{Y}\rho\mathbf{Y} + p_3\mathbf{Z}\rho\mathbf{Z}, \tag{1}$$

where the p_j terms are classical probabilities. Therefore a completely acceptable interpretation of Eq. (1) is one where with probability $(1 - p_1 - p_2 - p_3)$ no error happens to the wave function, and with probability p_j a Pauli $\mathbf{X}$, $\mathbf{Y}$, or $\mathbf{Z}$ error occurs for $j = \{1,2,3\}$, respectively. This error model is referred to by a variety of different names in the literature. Here we refer to it as the "stochastic Pauli error model." More generally, an error model can be generated with a larger set of gates than just Pauli gates, but where error gates are randomly inserted in a quantum circuit with classical probabilities. The key characteristic of all these stochastic error models is that the various error configurations all arise from classical probabilities, resulting in no interfering pathways between them.

Coherent errors, which can arise by over- or under-rotations of a quantum gate, were often called "inaccuracies" in the early literature on quantum error correction [14,15]. They cannot map to any stochastic error model as they result in a fully coherent evolution with multiple interfering pathways. Proving the existence of threshold in the presence of coherent errors thus requires one to consider the fully coherent sum of interfering fault paths (see, e.g., Sec. 8 in Ref. [7]). The impact of coherent errors has received renewed attention due to recent results confirming that such errors can be a more severe hurdle for fault tolerance than stochastic errors [16,17].

A more thorough, physics-based justification for when a stochastic error model is an appropriate approximation requires one to consider the entire system-bath interaction. Only when the bath state, entangled with a given error, is orthogonal to all other bath states is the stochastic error model truly appropriate [5,14]. Despite these fairly well-known results from the early literature on quantum error correction, the use of stochastic error models is still widely used in numerical simulations to calculate thresholds, including many results that have examined the accuracy of approximating various error channels by stochastic errors [18–23]. Of course, a significant reason for using this error model is that these types of errors can be efficiently simulated classically via the Gottesman-Knill theorem [24,25] if one restricts the set of gates to the Clifford group or a subset (often just Pauli operators are used).

Here, we report that a stochastic error model has a drastically different logical failure distribution than a failure distribution resulting from coherent errors. To show this, we compare the output failure distributions of a quantum error correction (QEC) memory circuit correcting stochastic Pauli errors to coherent errors. We utilize a numerical simulation of the entire encoded wave function, and we examine the failure distribution of the logical state for the Steane [[7,1,3]] code and a distance 3 surface code. We devise failure metrics that avoid the need to implement a final round of perfect error correction and decoding, commonly used when studying the failure characteristics of a logical channel [18,22,23,26]. Our

---

[*] jeff.barnes@jhuapl.edu

results show that the output failure distributions are markedly different for the two error models, with coherent errors leading to very broad failure distributions. This suggests that outlier events are much more likely to occur for coherent errors than for stochastic errors, which may provide insight into why they can be so harmful to QEC [16,17].

II. NUMERICAL SIMULATION APPROACH

We numerically simulate two common $d = 3$ QEC codes in this paper: the Steane [[7,1,3]] code [2,10] and the [[9,1,3]] titled-13 surface code [27–29]. Insertions of errors in the stochastic Pauli (SP) error model are treated as unitary qubit gates, so for both the SP error model and the pulse-area error model the evolution is purely unitary in our simulator. The goal of the report is to determine and compare the output failure probability distributions between these two error models.

Each run starts with the following state:

$$|\Psi_0\rangle = (\cos\theta\,|0_L\rangle + \sin\theta\, e^{i\phi}|1_L\rangle) \otimes |0000\rangle. \tag{2}$$

Here, $\theta = \pi$ rand() and $\phi = 2\pi$ rand(), with rand() referring to a uniform pseudorandom number. This covers the Bloch sphere, though not necessarily uniformly.

A. Quantum operations

For a single qubit, the most general evolution is given by an interaction Hamiltonian,

$$\mathbf{H} = \hbar\omega(u_x\mathbf{X} + u_y\mathbf{Y} + u_z\mathbf{Z}), \tag{3}$$

where $\mathbf{X}$, $\mathbf{Y}$, and $\mathbf{Z}$ are Pauli operators [10], the rotation axis is (u_x,u_y,u_z), and couplings with field amplitudes are absorbed into ω. Evolution is given by $|\Psi\rangle \to \mathbf{U}|\Psi\rangle$, with the following propagator:

$$\begin{aligned}\mathbf{U} &= \exp(-i\mathbf{H}t/\hbar)\\ &= \cos(\omega t)\mathbf{1} - i\,\sin(\omega t)(u_x\mathbf{X} + u_y\mathbf{Y} + u_z\mathbf{Z}).\end{aligned} \tag{4}$$

In these simulations, the *shortest* path in Hilbert space is used to evolve a gate. Thus, the Hadamard gate $\mathbf{W} = (\mathbf{X} + \mathbf{Z})/\sqrt{2}$ is created with the axis $(1,0,1)/\sqrt{2}$ and the duration $t = \pi/(2\omega)$.

The controlled-NOT (CNOT) $(n \to m)$ gate is implemented using the following Hamiltonian:

$$\mathbf{H} = \hbar\omega(\mathbf{1} - |1_n\rangle\langle 1_n| + |1_n\rangle\langle 1_n| \otimes \mathbf{X}_m). \tag{5}$$

The projectors ensure that no phase difference accumulates for $|0_n\rangle$. This same structure extends to more than one controlling qubit, such as the Toffoli gate. For the controlled-Z gate, replace $\mathbf{X}$ with $\mathbf{Z}$.

A measurement of qubit n is implemented as

$$|\Psi\rangle \to \begin{cases} |0_n\rangle\langle 0_n|\Psi\rangle/\|\langle 0_n|\Psi\rangle\| & \text{rand()} \leqslant |\langle 0_n|\Psi\rangle|^2,\\ |1_n\rangle\langle 1_n|\Psi\rangle/\|\langle 1_n|\Psi\rangle\| & \text{otherwise.}\end{cases} \tag{6}$$

Measurements are instantaneous, and their records are perfect. These are standard assumptions in QEC.

B. Error models

1. *Pauli error model*

A stochastic Pauli error model is implemented by selecting a set of fault locations and an error rate, p. A detailed discussion can be found in Ref. [30]. The choice here is conservative: errors are restricted to being only on the codeword qubits and only before each syndrome measurement. While conservative, this is not unrealistic for this error model as the Pauli errors can be efficiently commuted through a QEC circuit. When the code encounters a fault location, it randomly applies an $\mathbf{X}$ error and a $\mathbf{Z}$ error each with probability p. Since $\mathbf{XZ} = -i\mathbf{Y}$, all Pauli errors can occur.

2. *Pulse-area error model*

For coherent errors, we utilize an error model that we call the pulse-area error model. Coherent manipulations of quantum systems almost universally involve the application of an electromagnetic field, and these are imprecise. Static fields are not independent degrees of freedom, and their fluctuations are tied back to their sources [31,32]. Free fields, which include RF pulses in magnetic resonance [33] and laser pulses in time domain optical spectroscopy [34], are usually well represented by coherent states [35], and their quantum back-action is quantifiable [36]. Commonly, though, these terms can be neglected, and the field amplitudes are c functions in the Hamiltonian that describes a qubit gate. A perfect gate requires the integral of the field amplitude over time (in a rotating frame) to be a fixed angle. The pulse-area error model puts a distribution on this angle. The mean is zero, since systematic errors can be removed with calibration [37].

The pulse-area error model consists of replacing ω in Eq. (4) with $\omega(1 + \sigma r)$, with $-1 < r < 1$ uniformly and independently per gate:

$$\exp\left(-\frac{i}{\hbar}[\hbar\omega\mathbf{G}]\frac{\pi}{2\omega}\right) \to \exp\left(-\frac{i}{\hbar}[\hbar(1+\sigma r)\mathbf{G}]\frac{\pi}{2}\right). \tag{7}$$

All gates in the QEC circuit have $\omega = 1.0$ and a duration of $\pi/2$. Thus, σ is related to the fractional jitter in the field amplitudes.

III. METRIC FOR QEC FAILURE

This section derives a metric to quantify QEC circuit failure, but adapted to a wavefunction simulation. The prescription here is for the Steane [[7,1,3]] code with a few special considerations required for the surface code noted in Sec. III B. The focus here is on developing a metric for failure that does not require any perfect measurements, QEC rounds, or decoding, but rather a metric that can be applied to the wave function itself.

A. Steane failure metric

The following definition, from Ref. [6], is considered a standard: a QEC circuit that takes any input state with weight $\leqslant 1$ errors and outputs a state with weight $\leqslant 1$ errors has succeeded; otherwise it has failed. A weight-1 error is defined as having a single Pauli error applied to the state, a weight-2 error has two errors, and so on. The goal is to estimate the probability of failure $P_{\text{fail}}(p)$ over many trial runs at fixed p. The concatenation threshold is based upon the bound $P_{\text{fail}}(p) < p$ (but there are subtle corrections, see Ref. [6]).

This suggests measuring $P_{\text{fail}}(p)$ as the portion of $|\Psi(t)\rangle$ that projects into the space of all weight $\geqslant 2$ errors. There are several possibilities for this space. Consider using operators, as in a CNOT-Hadamard-Phase (CHP) simulation [25]. For example, the [[3,1,3]] bit-flip correcting code is constructed as in Eq. (8):

$$\begin{aligned}
\overbrace{T(2,3,1)C(1,2)C(1,3)}^{\text{repair}}\,\overbrace{X(1)}^{\text{error}}\,\overbrace{C(1,3)C(1,2)}^{\text{encode}}\,\overbrace{P(2,3)}^{\text{ancilla}} &= X(2)X(3)P(2,3),\\
T(2,3,1)C(1,2)C(1,3)\; X(2)\; C(1,3)C(1,2)\; P(2,3) &= X(2)P(2,3),\\
T(2,3,1)C(1,2)C(1,3)\; X(3)\; C(1,3)C(1,2)\; P(2,3) &= X(3)P(2,3),
\end{aligned} \tag{8}$$

where T and C denote Toffoli and CNOT gates, respectively. The P is a projector to $|0\rangle$ that enforces the requirement of fresh ancilla. Any bit-flip error between the encoding and repair steps, by simple matrix multiplication, is seen to never act on qubit 1. This proves the QEC circuit protects the qubit. The point is that $|\Psi_0\rangle$ does not appear anywhere in this proof. This suggests the QEC failure space for a $d = 3$ code is built up from the logical codeword space, as in Eq. (9):

$$\begin{aligned}
\mathcal{S}_L = \{|0_L\rangle,\, |1_L\rangle\},\quad \mathcal{S}_{L+1} &= \mathcal{S}_L \cup \{\mathbf{X}_q|0_L\rangle,\, \mathbf{X}_q|1_L\rangle,\, \mathbf{Y}_q|0_L\rangle,\, \mathbf{Y}_q|1_L\rangle,\, \mathbf{Z}_q|0_L\rangle,\, \mathbf{Z}_q|1_L\rangle\},\\
\mathcal{S}_{L+2} = \mathcal{S}_L \cup \{\mathbf{X}_q|0_L\rangle,\, \mathbf{X}_q|1_L\rangle,\, &\mathbf{Z}_q|0_L\rangle,\, \mathbf{Z}_q|1_L\rangle,\, \mathbf{X}_q\mathbf{Z}_{q'}|0_L\rangle,\, \mathbf{X}_q\mathbf{Z}_{q'}|1_L\rangle\}\quad \forall q,q'.
\end{aligned} \tag{9}$$

These kets form orthonormal states, with $|\mathcal{S}_L| = 2$, $|\mathcal{S}_{L+1}| = 44$, and $|\mathcal{S}_{L+2}| = 128$ for the particular case of the Steane code. Further, since $\mathbf{X}_q\mathbf{Z}_q = -i\mathbf{Y}_q$, one can show $\mathcal{S}_L \subset \mathcal{S}_{L+1} \subset \mathcal{S}_{L+2}$. But note that the total Hilbert space of the Steane code has $2^7 = 128$ dimensions. Thus, $\mathcal{S}_{L+2}$ completely spans it. Since no state could ever leave $\mathcal{S}_{L+2}$, it cannot represent a QEC failure criteria, but $\mathcal{S}_{L+1}$ can.

From the vantage point of Monte Carlo wave-function simulations, it seems more natural to check if two or more Pauli operators have acted on the starting state $|\Psi_0\rangle$ for a $d = 3$ code. These spaces are built up as

$$\begin{aligned}
\mathcal{S}_\psi &= \{|\Psi_0\rangle\},\\
\mathcal{S}_{\psi+1} &= \mathcal{S}_\psi \cup \{\mathbf{X}_q|\Psi_0\rangle,\, \mathbf{Y}_q|\Psi_0\rangle,\, \mathbf{Z}_q|\Psi_0\rangle\},\\
\mathcal{S}_{\psi+2} &= \mathcal{S}_\psi \cup \{\mathbf{X}_q|\Psi_0\rangle,\, \mathbf{Z}_q|\Psi_0\rangle,\, \mathbf{X}_q\mathbf{Z}_{q'}|\Psi_0\rangle\}.
\end{aligned} \tag{10}$$

They are orthonormal sets, with $|\mathcal{S}_{\psi+1}| = 22$ and $|\mathcal{S}_{\psi+2}| = 64$ for the particular case of the Steane code. Since the Steane code and the surface code are both Calderbank-Shor-Steane (CSS) codes, they correct errors of the form $\mathbf{X}_q\mathbf{Z}_{q'}$ for all q and q'. Checking if $|\Psi(t)\rangle$ has ventured beyond either $\mathcal{S}_{\psi+1}$ or $\mathcal{S}_{\psi+2}$ is reasonable.

To summarize, we have three metrics to detect a QEC circuit failure:

$$\begin{aligned}
P_{\text{fail}}^{(L+1)} &= 1 - \sum_{s\in L+1} |\langle s|\Psi(t)\rangle|^2,\\
P_{\text{fail}}^{(\psi+2)} &= 1 - \sum_{s\in\psi+2} |\langle s|\Psi(t)\rangle|^2,\\
P_{\text{fail}}^{(\psi+1)} &= 1 - \sum_{s\in\psi+1} |\langle s|\Psi(t)\rangle|^2.
\end{aligned} \tag{11}$$

For each simulation, when they are 1, the circuit has failed; otherwise, we expect them to be 0. Technically the sums in Eq. (11) should also extend over the ancilla qubits. However, we assume that measurements are perfect; therefore when we analyze the failure metrics, we know that the ancilla will be in a product state with the data qubits, and thus the sum over them is independent and can be excluded.

Two additional metrics are useful: the projection onto $\mathcal{S}_L$, given in Eq. (12), and the fidelity $\mathcal{F}$, in Eq. (13):

$$P_{\text{code}} = \sum_{s\in\mathcal{S}_L} |\langle s|\Psi(t)\rangle|^2, \tag{12}$$

$$\mathcal{F}^2 = |\langle\Psi(t)|(\alpha|0_L\rangle + \beta|1_L\rangle)|^2. \tag{13}$$

The result $\mathcal{F} = 1.0$ implies a perfect repair.

Several useful bounds are as follows:

$$\begin{aligned}
P_{\text{fail}}^{(L+1)} &\leqslant P_{\text{fail}}^{(\psi+1)},\\
P_{\text{fail}}^{(\psi+2)} &\leqslant P_{\text{fail}}^{(\psi+1)},\\
\mathcal{F}^2 \leqslant P_{\text{code}} &\leqslant 1 - P_{\text{fail}}^{(L+1)}.
\end{aligned} \tag{14}$$

Physically, a low P_{code} implies a low $\mathcal{F}$, since $|\Psi(t)\rangle$ is outside of $\mathcal{S}_L$. The inverse does not hold, since a logical error such as $|1_L\rangle = \mathbf{X}_L|0_L\rangle$ on an encoded $|0_L\rangle$ leaves $P_{\text{code}} = 1$ but $\mathcal{F} = 0$. It is also seen that $P_{\text{fail}}^{(\psi+1)}$ is the most stringent criteria for circuit failure.

Several computational tools to Monte Carlo estimate a pseudothreshold apparently restrict $|\Psi_0\rangle$ to be one of the six stabilizer states:

$$\{|0_L\rangle, |1_L\rangle, (|0_L\rangle \pm |1_L\rangle)/\sqrt{2}, (|0_L\rangle \pm i|1_L\rangle)/\sqrt{2}\}. \tag{15}$$

This makes drawing distinctions between the metrics in Eq. (11) problematic, as discussed later in this paper.

B. Surface code failure metric

The failure metrics for the Steane code were relatively straightforward since all errors map to a unique syndrome. There is a degeneracy in the surface code that complicates this somewhat. We show here how to define a failure metric analogous to that for the Steane code that takes this into account.

TABLE I. The six syndromes for the Steane [[7,1,3]] code, in the left-hand column. The right-hand columns show the errors they detect.

Operator	$\mathbf{Z}_1$	$\mathbf{Z}_2$	$\mathbf{Z}_3$	$\mathbf{Z}_4$	$\mathbf{Z}_5$	$\mathbf{Z}_6$	$\mathbf{Z}_7$
$\mathbf{X}_2\mathbf{X}_4\mathbf{X}_5\mathbf{X}_7$	0	1	0	1	1	0	1
$\mathbf{X}_3\mathbf{X}_4\mathbf{X}_5\mathbf{X}_6$	0	0	1	1	1	1	0
$\mathbf{X}_1\mathbf{X}_4\mathbf{X}_6\mathbf{X}_7$	1	0	0	1	0	1	1
Operator	$\mathbf{X}_1$	$\mathbf{X}_2$	$\mathbf{X}_3$	$\mathbf{X}_4$	$\mathbf{X}_5$	$\mathbf{X}_6$	$\mathbf{X}_7$
$\mathbf{Z}_2\mathbf{Z}_3\mathbf{Z}_6\mathbf{Z}_7$	0	1	1	0	0	1	1
$\mathbf{Z}_1\mathbf{Z}_3\mathbf{Z}_5\mathbf{Z}_7$	1	0	1	0	1	0	1
$\mathbf{Z}_1\mathbf{Z}_2\mathbf{Z}_3\mathbf{Z}_4$	1	1	1	1	0	0	0

The logical state is generated utilizing the parity-check matrix constructed from the $\hat{X}$ stabilizers for the surface code shown later in Eq. (22). It results in the basis states:

$$\begin{aligned}
|0\rangle_L = {} & \tfrac{1}{4}(|000000000\rangle + |110110000\rangle + |011000000\rangle \\
& + |101110000\rangle + |000000110\rangle + |110110110\rangle \\
& + |011000110\rangle + |101110110\rangle + |000011011\rangle \\
& + |110101011\rangle + |011011011\rangle + |101101011\rangle \\
& + |000011101\rangle + |110101101\rangle + |011011101\rangle \\
& + |101101101\rangle), \\
|1\rangle_L = {} & \hat{X}^{\otimes 9} |0\rangle_L ,
\end{aligned} \tag{16}$$

which we can use to construct our logical code space as in Eq. (9). Note that state $|1\rangle_L$ is the $|0\rangle_L$ state under the action of the bitwise-NOT on every binary string within its sum. Due to this relation, there is an equivalence in the action of single-qubit errors to both $|0\rangle_L$ and $|1\rangle_L$ with respect to the degeneracy of the single-error spaces. For single-qubit errors, there is equivalence of the action of $\hat{X}$ errors, $\hat{X}_1 |0\rangle_L = \hat{X}_2 |0\rangle_L$ and $\hat{X}_6 |0\rangle_L = \hat{X}_7 |0\rangle_L$, and also degeneracies for $\hat{Z}$ errors, $\hat{Z}_0 |0\rangle_L = \hat{Z}_3 |0\rangle_L$ and $\hat{Z}_5 |0\rangle_L = \hat{Z}_8 |0\rangle_L$. $\hat{Y}$ errors are completely nondegenerate. We can therefore construct the failure criteria pertaining to the logical codeword space in the following manner:

$$\begin{aligned}
\mathcal{S}_L &= \{|0\rangle_L , |1\rangle_L\}, \\
\mathcal{S}_{L+1} &= \mathcal{S}_L \cup \{\hat{X}_i |0\rangle_L , \hat{X}_i |1\rangle_L , \hat{Y}_j |0\rangle_L , \hat{Y}_j |1\rangle_L , \\
& \quad \times \hat{Z}_k |0\rangle_L , \hat{Z}_k |1\rangle_L\} \text{ s.t. } i \neq 2,7;\ k \neq 3,8,
\end{aligned} \tag{17}$$

where the indices i, j, and k run over all data qubit indices unless otherwise specified. Similarly, for the criteria more natural for the purpose of wave-function simulations the spaces can be constructed as

$$\begin{aligned}
\mathcal{S}_\psi &= \{|\Psi_0\rangle\}, \\
\mathcal{S}_{\psi+1} &= \mathcal{S}_\psi \cup \{\hat{X}_i |\Psi_0\rangle , \hat{Y}_j |\Psi_0\rangle , \hat{Z}_k |\Psi_0\rangle\}, \\
\mathcal{S}_{\psi+2} &= \mathcal{S}_\psi \cup \{\hat{X}_i |\Psi_0\rangle , \hat{Z}_k |\Psi_0\rangle , \hat{X}_i\hat{Z}_k |\Psi_0\rangle\}, \\
& \qquad \text{such that } i \neq 2,7;\ k \neq 3,8,
\end{aligned} \tag{18}$$

where, again, the indices run over all qubits except for special cases. While it appears that some single-qubit $\hat{Y}$ errors have been omitted in the space $\mathcal{S}_{\psi+2}$, the symmetry of the error space ensures that these states have been taken into account. For instance, the state $\hat{Y}_2 |\Psi_0\rangle = i\hat{X}_2\hat{Z}_2 |\Psi_0\rangle$, which, through the degeneracy of the $\hat{X}$ errors, can be represented by the state $i\hat{X}_1\hat{Z}_2 |\Psi_0\rangle$. The assessment of the surface code will incorporate computing the overlap of output wave functions with the aforementioned correctable error spaces. Because the surface code is an error correcting code, the sucess criteria P_{code} and fidelity ($\mathcal{F}^2$) given in Eqs. (12) and (13) will be of interest as well.

IV. STEANE SIMULATION RESULTS

With failure criteria now defined, we proceed to simulate the error models discussed in Sec. II B for the Steane [[7,1,3]] code. The baseline QEC trial begins by encoding a random qubit. The syndromes, and the errors they detect, are given in Table I. To ensure fault tolerance, the three syndromes that check for **Z** errors are measured and then measured again. A loop back occurs if the three sets of syndrome bits do not match. Otherwise, any **Z** errors are repaired, and the circuit repeats this for the **X**-error-detecting syndromes.

The syndrome measurement procedure uses Shor style ancilla. It begins by creating a cat state in the four ancilla qubits, which is always error free. The test and rejection steps seen in Fig. 6 of Ref. [6] are thus not required. After entanglement, the cat state is rotated and read out in the style discussed in Ref. [38]. Each ancilla is then perfectly reinitialized allowing them to be reused for the next syndrome.

A. Pauli error model

The Steane QEC circuit was run 3×10^6 times at nine different p values. Histograms of each failure criteria are shown in Fig. 1. The metric $P_{\text{fail}}^{(L+1)}(p)$ is binominally distributed (within numerical accuracy) and has the obvious interpretation. The fraction of trials with $P_{\text{fail}}^{(L+1)}(p) = 1$ for a given p is shown by the red curve in Fig. 2. A pseudothreshold of $\approx$0.005 can be observed. The curve appears similar to examples provided in Ref. [39] and gives confidence that the wave-function simulations can reproduce the standard pseudothreshold.

The difficulty with $P_{\text{fail}}^{(\psi+1)}$ and $P_{\text{fail}}^{(\psi+2)}$ is that the spaces of Eq. (10) are not aligned with the six stabilizer states of Eq. (15). When the code is run with the $|\Psi_0\rangle$ restricted to be from the set of Eq. (15), then all three metrics in Eq. (11) are binomially distributed. We note here that all Gottesman-Knill and error propagation simulations either require or implicitly assume that input states are stabilizer states. Even for Pauli errors, this restriction already changes the output failure distribution away from what will actually happen when arbitrarily encoded

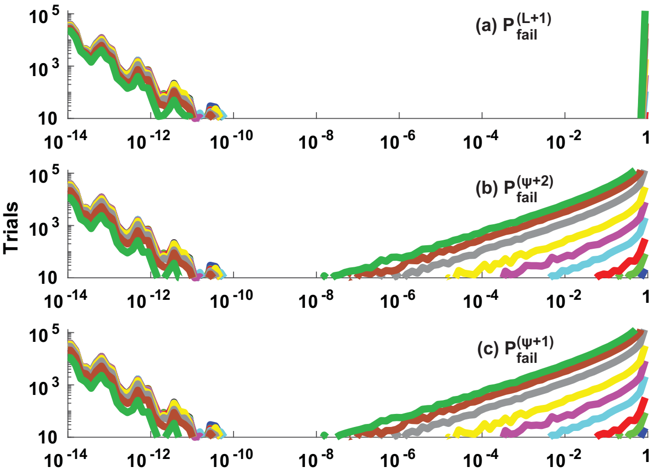

FIG. 1. Histograms of the Steane QEC failure metrics, from 3×10^6 trials of the Steane QEC circuit, using the Pauli error model with $p = 0.00005, 0.0001, 0.0002, 0.0005, 0.001, 0.002, 0.005, 0.01, 0.02$. $P^{(L+1)}_{\rm fail}$ (a) is always binomially distributed, but $P^{(\psi+2)}_{\rm fail}$ (b) and $P^{(\psi+1)}_{\rm fail}$ (c) never are.

states must be protected. Since arbitrary encoded states cannot be abandoned, how can this result be understood?

First ask the following: does *every* nonzero value of $P^{(\psi+1)}_{\rm fail}$ or $P^{(\psi+2)}_{\rm fail}$ indicate a circuit failure? One way to examine this is to run chains of QEC circuits, where the input of the next QEC cycle is the output of the previous one. In such simulations, $P_{\rm code}$ and $\mathcal{F}$ transiently drop from 1.0, but then they recover, as seen in Fig. 3(a). This is a case where weight-1 errors escape a QEC cycle, only to be repaired in the next cycle. By chance, this can occur sequentially, but the $P_{\rm fail}$ metrics remain 0.0, indicating the errors were not fatal ones.

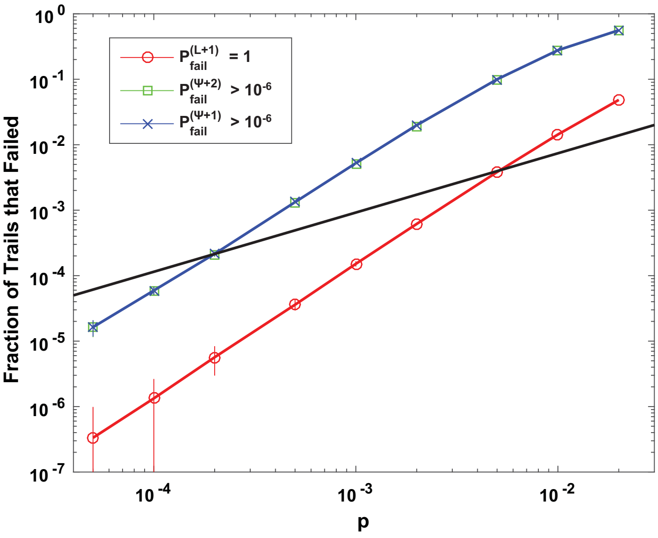

FIG. 2. The Monte Carlo simulation of the failure rate for the Steane QEC circuit, using the Pauli error model. The red circles are the fraction of trials with $P^{(L+1)}_{\rm fail} = 1$. The blue and green symbols mark estimates of failure, based on the criteria of $P^{(\psi+2)}_{\rm fail} > 10^{-6}$ and $P^{(\psi+1)}_{\rm fail} > 10^{-6}$. The vertical bars represent the 95% confidence level in the estimates. The black line marks the pseudothreshold criteria of $P_{\rm fail}(p) = p$.

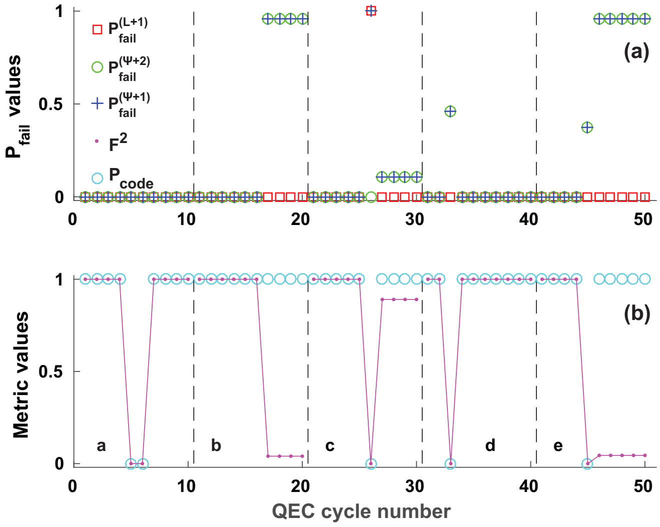

FIG. 3. Shown are five different runs of ten consecutive cycles of the Steane [[7,1,3]] QEC circuit, using the Pauli error model. (a) Plots of the three metrics for QEC failure under consideration. (b) Plots of $\mathcal{F}^2$ and $P_{\rm code}$.

In contrast, if $\mathcal{F}^2 < 1$ and $P_{\rm code} = 1$, then the encoded qubit was corrupted, and clearly the QEC circuit failed. These situations are seen in Figs. 3(b) to 3(e). Scatter plots of large samples with $p = 0.02$ did not find any other distinct behaviors, so we consider how to explain each case.

1. *Case b*

Within a single cycle, $P_{\rm code} = 1$ and $\mathcal{F} < 1$, indicating a corrupted but encoded qubit. There are many insertions of three Pauli errors that caused this. An example is $\mathbf{X}_4$, $\mathbf{X}_5$, and then $\mathbf{X}_6$, all during the measurement of the $\mathbf{Z}$-error-detecting syndromes. Within the Steane code, $\mathbf{X}_5\mathbf{X}_4 \equiv \mathbf{X}_6\mathbf{X}_L$, so the $\mathbf{X}$ repair returns $\mathbf{X}_L|\Psi_0\rangle$, a properly encoded but corrupted state.

In the failed QEC cycle, it is found that $P^{(L+1)}_{\rm fail} = 0$, yet $P^{(\psi+2)}_{\rm fail} = P^{(\psi+1)}_{\rm fail} = 0.9597$ and $\mathcal{F} = 0.2008$. The explanation comes by considering the starting state of Eq. (2). For a $\mathbf{X}_L$ error, $P^{(\psi+1)}_{\rm fail} = 1 - \sin^4\theta\,\cos^2\phi$. If the success criteria is set by demanding a threshold, say $P^{(\psi+1)}_{\rm fail} > 10^{-6}$, then irreparable errors are allowed when encoded states are "lucky" enough to be nearly an eigenstate of that error. For a threshold of 10^{-6}, errors are allowed if they shift $|\Psi_0\rangle$ by $< 0.05^\circ$ on the Bloch sphere. Whether this suffices will depend on the needs of the quantum algorithm.

2. *Case c*

In this trial, two fault locations had errors. Referring to Table I, the $\mathbf{Z}$ error detection syndromes finished without errors, but a $\mathbf{Z}_6$ error occurs after the first two $\mathbf{X}$ syndrome measurements. Since these are checking for $\mathbf{X}$ errors, the syndrome is (0,0,0). In the second round, a $\mathbf{X}_7$ error occurs before the last syndrome. This error should return (1,1,0), but we are on the last syndrome, so (0,0,0) results. As the consistency check is passed, no errors are detected. For this p^2 process, an error of $\mathbf{X}_7\mathbf{Z}_6$ escapes. These combinations of $\mathbf{X}_q\mathbf{Z}_{q'}$ for $q \neq q'$ are the only errors that distinguish $P^{(\psi+1)}_{\rm fail}$

from $P_{\text{fail}}^{(\psi+2)}$. In the spirit of Ref. [6], the more stringent weight-1 error criteria of $P_{\text{fail}}^{(\psi+1)} > 10^{-6}$ is favored.

3. Cases d and e

This appears to show cases where $P_{\text{fail}}^{(\psi+1)} > 10^{-6}$ cannot distinguish all errors. Both cases (d) and (e) would be detected as errors, yet the permanent loss of $\mathcal{F}$ in case (d) is not observed in case (e). An examination of several QEC chain trials suggests the answer.

In one case, during the second measurement of the syndromes to detect $\mathbf{X}$ errors, but just before the consistency check, the following Pauli operators were inserted: S, $\mathbf{X}_5$, S, $\mathbf{X}_6$, S, where S implies a syndrome measurement. The first syndrome returns 0. An $\mathbf{X}_5$ error should give (1,0,0), so the second syndrome returns 0. At the next error, $\mathbf{X}_6\mathbf{X}_5 \equiv \mathbf{X}_4\mathbf{X}_L$, and the syndrome for an $\mathbf{X}_4$ error is (0,1,0). Thus, the last measurement yields (0,0,0), consistent with the first syndrome measurments. This p^2 process allowed a corrupted qubit with a weight-1 error to pass.

In another case, in the second measurement of the $\mathbf{X}$ error detecting syndromes, this sequence was found: S, $\mathbf{X}_3$, S, $\mathbf{X}_2$, S. As before, this dances around the detection table, and $\mathbf{X}_6\mathbf{X}_L$ escapes. In the next QEC cycle, however, a single $\mathbf{X}_3$ error occurs within the $\mathbf{Z}$-detecting syndromes. Only a $\mathbf{X}_2$ error is left for the QEC circuit to repair. By random chance, a p process has fixed an unrepairable p^2 error.

Three cases involving p^2 processes with outcomes like in case (e) were examined. They all had the same result: by random chance, the next QEC cycle had a p process that converted the weight-2 error into a weight-1 error. As this cannot be assigned to the role of the QEC circuit, we favor the criteria $P_{\text{fail}}^{(\psi+1)} > 10^{-6}$ to be a good detector of QEC circuit failure.

B. Pulse-area error model

We now use the pulse-area error model outlined in Eq. (7). The reader should keep in mind the following argument in support of a stochastic error model. Consider the QEC circuit as an operator expansion:

$$\cdots \mathbf{U}_5\mathbf{U}_4\Omega_3\mathbf{U}_2\mathbf{U}_1|\Psi_0\rangle. \tag{19}$$

There are measurements Ω and unitary gates $\mathbf{U}$. Following Eq. (7), and using $\mathbf{U}_n^2 = \mathbf{1}$, this becomes

$$\cdots \Omega_3\left(\cos\frac{\pi\sigma r_2}{2}\,\mathbf{U}_2 - i\sin\frac{\pi\sigma r_2}{2}\,\mathbf{1}\right) \times\left(\cos\frac{\pi\sigma r_1}{2}\,\mathbf{U}_1 - i\sin\frac{\pi\sigma r_1}{2}\,\mathbf{1}\right)|\Psi_0\rangle. \tag{20}$$

Now suppose $\sigma \ll 1$. In that case, the linear terms in σ simply have each gate $\mathbf{U}_n \to \mathbf{1}$. This superficially resembles the Pauli error model: insert a Pauli operator, which cancels the gate, with amplitude σr_n at gate n. The *sum* of these terms in Eq. (20) creates $|\Psi(t)\rangle$. Using the argument in support of the stochastic error model, each syndrome measurement Ω selects one of these terms at a time, so the incoherent sum only needs to be considered. That is very useful, because even if $\sigma^2 \ll \sigma$, with the 144 gates of the Steane syndrome extraction circuitry, there are 10 296 dual gate $O(\sigma^2)$ terms to add up, which would be difficult. Yet, in order to fully select one error, six syndromes must be measured, even while errors continue to accumulate. The numerical simulation can be used to check this approximation.

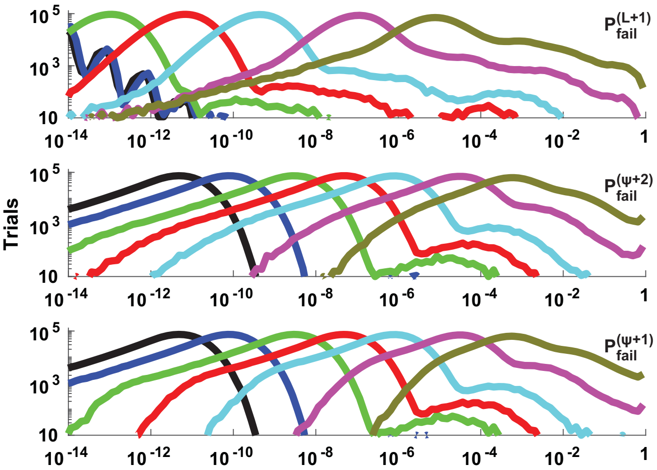

FIG. 4. Histograms of the Steane QEC circuit failure metrics, for 1×10^6 trials of $\sigma = 0.001$, 0.002, 0.005, 0.010, 0.020, 0.050, and 0.100. The curves proceed from left to right in the bottom panel.

To see how the Steane code handles these pulse-area errors, 10^6 trials with $0.001 \leqslant \sigma \leqslant 0.100$ are shown in Fig. 4. All three failure metrics are shown for completeness. First, note that the distributions are *very* broad. A curve fit to the distribution of $P_{\text{fail}}^{(\psi+1)}(\sigma = 0.01)$ showed that roughly 75% of the trials could be described by the log-normal distribution of the form $\exp[-a\log^2(bP_{\text{fail}})]$. The maximum likelihood scales as $\text{ML}(P_{\text{fail}}^{(\psi+1)}) \approx 5\sigma^4$. Employing the $P_{\text{fail}}^{(\psi+1)} > 10^{-6}$ critera for failure results in a failure-versus-σ curve in Fig. 5. For small σ, it varies as $\approx 200\sigma^{2.5}$, but comparison with Fig. 2 reveals a much more sigmodial shape.

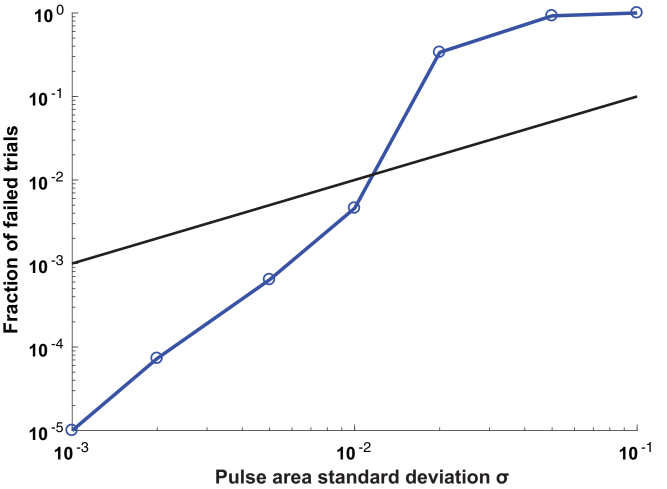

FIG. 5. Using the criteria $P_{\text{fail}}^{(\psi+1)} > 10^{-6}$ on the 10^6 trials of the Steane QEC circuit, under the pulse-area error model, gives rise to this failure rate curve. The failure rate does not follow the expected linear slope. The black line is the unit line.

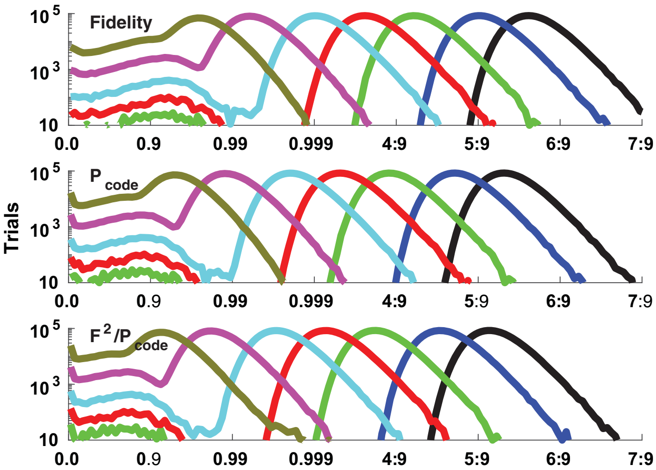

FIG. 6. The success metrics $\mathcal{F}$, P_{code}, and the ratio, for the pulse-area error model, acting on the Steane [[7,1,3]] QEC circuit. Values of σ correspond to those of Fig. 4.

In the Pauli error model, a successful QEC cycle competely restores the encoded qubit. What about the pulse-area error model? Figure 6 shows log-log plots for the distributions of $\mathcal{F}$ and P_{code}. Perfect outcomes ($\mathcal{F} = P_{\text{code}} = 1$) are not apparent, but it may be that the part of $|\Psi(t)\rangle$ outside of $\mathcal{S}_L$ is still repairable. What about the part inside? Consider the metric in Eq. (21):

$$\mathcal{F}^2/P_{\text{code}} = \frac{|\langle\Psi_0|\Psi(t)\rangle|^2}{|\langle 0_L|\Psi(t)\rangle|^2 + |\langle 1_L|\Psi(t)\rangle|^2}. \tag{21}$$

It normalizes the part of $|\Psi(t)\rangle$ still in $\mathcal{S}_L$. If it is < 1.0, then $|\Psi(t)\rangle$ has rotated from $|\Psi_0\rangle$ within the codeword space. This is an unrepairable error. Histograms of this metric are shown at the bottom of Fig. 6. For $\sigma = 0.005$, the most likely value of $\mathcal{F}^2/P_{\text{code}} \approx 0.0001$. Thus, a quantum calculation that encodes digital numbers into amplitudes will only be accurate to approximately 4 digits. This distribution scales like $4.6\sigma^4$, so to achieve float64 precision (16 decimal digits) requires $\sigma \approx 0.00007$. This is analogous to round-off errors in finite precision classical computers. We note that this error is likely to be reduced as code distance is increased, but lacking a distance 5 simulation we cannot show this.

We finally note that, like the Pauli error model, we have simulated strings of QEC circuits to examine the long-term behavior (not shown). This small errors noted here did not grow over multiple cycles, but remained bounded. The QEC circuit is working, but the behavior is much more complicated than the Pauli error model suggests.

V. SURFACE CODE SIMULATION RESULTS

We have demonstrated that the failure distributions for the pulse-area error model are qualitatively different than those generated by purely Pauli errors. For completeness we run a similar analysis on a surface code simulation. The particular variant we choose is the tilted-13 surface code, which is a variation on the distance 3 surface code that requires less data and ancilla qubits compared to conventional distance 3 surface code [27–29]. A diagram of the qubit and stabilizer layout of the code is shown in Fig. 7. The following is a list of the eight stabilizers:

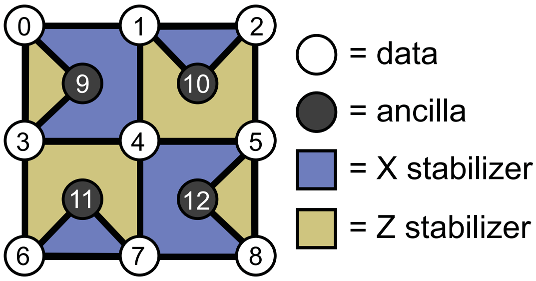

FIG. 7. The tilted-13 surface code (distance 3). A 3 × 3 layout of data qubits and a set of weight-2 and weight-4 stabilizers that, with an appropriate circuit schedule, is a fault-tolerant implementation of an error correcting code.

$$\begin{gathered}\hat{X}_0\hat{X}_1\hat{X}_3\hat{X}_4, \quad \hat{Z}_0\hat{Z}_3, \hat{X}_1\hat{X}_2, \quad \hat{Z}_1\hat{Z}_2\hat{Z}_4\hat{Z}_5, \hat{X}_6\hat{X}_7,\\ \hat{Z}_3\hat{Z}_4\hat{Z}_6\hat{Z}_7, \quad \hat{X}_4\hat{X}_5\hat{X}_7\hat{X}_8, \quad \hat{Z}_5\hat{Z}_8.\end{gathered} \tag{22}$$

The measurement of the weight-4 stabilizers is scheduled in such a way that single-qubit errors on the ancilla qubits propagate to, at most, two-qubit errors on the data in a manner such that the propagation direction is perpendicular to the direction of the logical operator of the surface code resulting in fault tolerance [40]. An additional requirement for fault tolerance is the repetitive measurement (typically for d measurement rounds) of the stabilizers before applying a correction operation.

For this study, a lookup table decoder was implemented for error correction [40]. This method utilizes a small set of syndrome processing rules that is equivalent to applying a minimum-weight perfect-matching algorithm [41–43] to only nearest-neighbor syndrome pairs [40] which, for a distance 3 code, is sufficient for error correction. There is some freedom to how one can schedule the syndrome extraction routine. For this manuscript we use a "single-shot" detection and correction cycle where we perform $\hat{X}$ followed by $\hat{Z}$ stabilizer measurements, repeat them three times to ensure fault tolerance, and then decoding and correction is performed once.

A. Pauli error model

The "single-shot" error correction routines were each run 1×10^6 times at each error rate: $p = 0.000001$, 0.0000025, 0.000005, 0.0000075, 0.00001, 0.000025, 0.00005, 0.000075, 0.0001, 0.0002, 0.0004, 0.0006, and 0.0008. We show the failure histograms generated from the surface code simulations in Fig. 8. Besides slightly shifted values for the failure histograms there is no qualitative difference between the surface code results compared to the Steane code shown in Fig. 1. This is not a surprising or unexpected result.

We observe a pseudothreshold of $\sim 3 \times 10^{-5}$ from these surface code simulations. Note that our reported pseudothresholds appear to be below the value reported in Ref. [40] of 3×10^{-4}. The simulations in Ref. [40] implement $|0\rangle_L$ as in input wave function while our simulations randomly sample a vector in the logical codeword space $1/\sqrt{2}(\alpha\,|0\rangle_L + \beta\,|1\rangle_L)$.

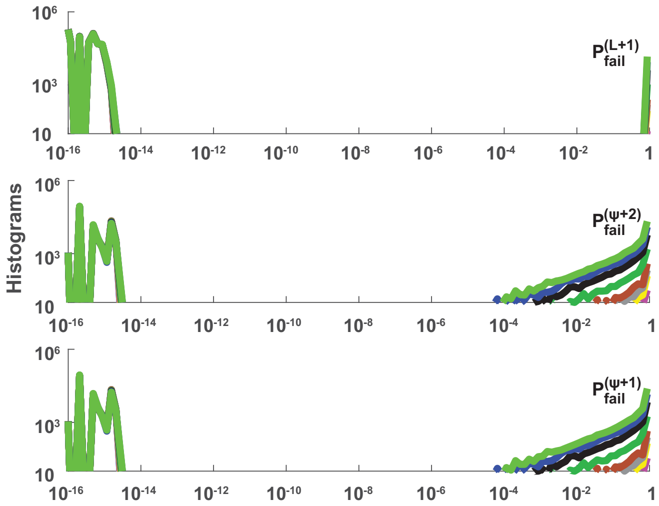

FIG. 8. Histograms of the failure criteria for the tilted surface code with the Pauli error model. 1×10^6 samples were accumulated per error rate. Pauli error rates: $p = 0.000001, 0.0000025, 0.000005, 0.0000075, 0.00001, 0.000025, 0.00005, 0.000075, 0.0001, 0.0002, 0.0004, 0.0006$, and 0.0008 generate the curves from left to right, respectively.

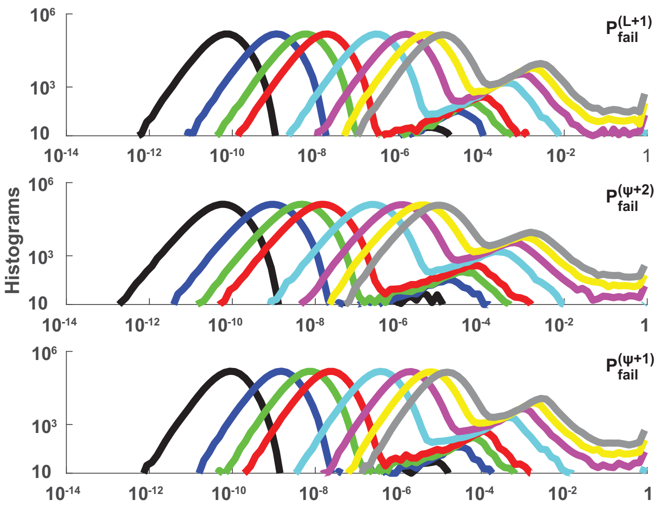

FIG. 9. Histograms of the failure criteria for the tilted surface code with the pulse-area error model. 1×10^6 samples were accumulated per error rate. Pulse area error strengths: $\sigma = 0.0025, 0.005, 0.0075, 0.01, 0.02, 0.03, 0.04$, and 0.05 generate the curves from left to right.

Also, there is a discrepancy between the labeling of the error rates between this study and the study in Ref. [40] where our recorded value of p is equivalent to $p/3$ in Ref. [40]. By fixing our initial state to just $|0\rangle_L$ and using the $P_{\rm fail}^{(L+1)}$ criteria, we obtain a pseudothreshold of $\approx 4 \times 10^{-5}$ which, in the language of Ref. [40], is reported as $p_{\rm th} \approx 1.2 \times 10^{-4}$; a comparable value.

B. Pulse-area error model

To compare the failure criteria of the surface code between the Pauli error model and the pulse-area error model, we perform surface code simulations using the exact same circuit as for the Pauli error model just shown. We use the following error strengths: $\sigma = 0.0025, 0.005, 0.0075, 0.01, 0.02, 0.03, 0.04$, and 0.05 (1×10^6 samples per error rate). Broad, heavy-tailed distributions for the failure criteria are again observed as shown in Fig. 9 and appear to follow a log-normal distribution in a majority of the cases. Once again, just as the failure metrics for the Pauli error model and the pulse-area error model varied drastically with the Steane code, the surface code displays similar behavior. There is no simple map between the Pauli error model and the pulse-area error model, with the pulse-area error model leading to quite broad and heavy-tailed distributions.

VI. CONCLUSIONS

We have presented a wave-function simulation of the Steane [[7,1,3]] quantum error correcting code and the tilted-13 surface code for both the stochastic Pauli error model and the coherent pulse-area error model for randomly encoded states. The usual failure criteria had to be modified in order to account for the different frame that nonstabilizer states occupy. A comparison of Figs. 1 and 4 shows that the two error models result in markedly different failure distributions. Pauli errors tend to draw $P_{\rm fail}^{\psi+1}(p)$ down from 1.0 with increasing p. These tails empirically vary as $\sqrt{P_{\rm fail}^{\psi+1}}$. In contrast, for increasing σ in the pulse-area error model, the distribution rises from small $P_{\rm fail}^{\psi+1}$, with the most likely values scaling as σ^4. We conjecture that the heavy tails in the pulse-area error model distribution are an indicator of the strongly negative impact that purely coherent errors can have on QEC [16,17].

These results also demonstrate that any result attempting to approximate arbitrary physical error channels with stochastic Pauli error channels must do so only when modeling certain system-bath type models. We have shown that one cannot rely on the assumption that syndrome measurements cut off the interfering pathways. A stochastic error model is only appropriate when the source of noise is due only to errors that are entangled with bath states that are mutually orthogonal to all other bath states. Of course, this is not true in general with coherent errors being the extreme counterexample. A simulation employing such an approximation, while it may be able to bound or approximate a mean threshold, will not be able to reproduce the output distribution that contains information from the fully coherent sum of all fault paths. As we have shown here, even for very small perturbations, the coherent addition of these fault paths causes marked differences in the output statistics. This also implies that any analysis that contains a perfect QEC measurement cycle and correction will, by design, cut off these coherent pathways, also corrupting the output statistics.

Finally, we note that these output distributions can be used as a more robust metric for QEC performance than just considering the logical error rate. They would allow one to examine whether ideas to randomize coherent errors, such as randomized compiling [44], do indeed help by making the errors look more "Pauli" like to QEC. The authors do not expect to see any benefit from randomized compiling as the evolution for a single trajectory would still be completely coherent, but this is a question for further investigation.

ACKNOWLEDGMENTS

We acknowledge useful conversations with J. Hoffmann and K. Brown. This project was supported by the Intelligence Advanced Research Projects Activity via Department of Interior National Business Center Contract No. 2012-12050800010. The U.S. Government is authorized to reproduce and distribute reprints for Governmental purposes notwithstanding any copyright annotation thereon. The views and conclusions contained herein are those of the authors and should not be interpreted as necessarily representing the official policies or endorsements, either expressed or implied, of IARPA, DoI/NBC, or the U.S. Government.

---

[1] P. W. Shor, Phys. Rev. A **52**, R2493 (1995).
[2] A.M. Steane, Phys. Rev. Lett. **77**, 793 (1996).
[3] A. R. Calderbank and P. W. Shor, Phys. Rev. A **54**, 1098 (1996).
[4] D. Aharonov and M. Ben-Or, in *Proceedings of the Twenty-Ninth Annual ACM Symposium on Theory of Computing, STOC '97* (ACM, New York, 1997), pp. 176–188.
[5] E. Knill, R. Laflamme, and W. H. Zurek, Proc. R. Soc. London, Ser. A **454**, 365 (1998).
[6] P. Aliferis, D. Gottesman, and J. Preskill, Quantum Inf. Comput. **6**, 97 (2006).
[7] D. Aharonov and M. Ben-Or, SIAM J. Comput. **38**, 1207 (2008).
[8] D. Gottesman, in *Quantum Information Science and Its Contributions to Mathematics* (American Mathematical Society, Providence, 2010), pp. 13–58.
[9] B. M. Terhal, Rev. Mod. Phys. **87**, 307 (2015).
[10] M. A. Nielsen and I. L. Chuang, *Quantum Computation and Quantum Information*, 10th ed. (Cambridge University, Cambridge, England, 2010).
[11] F. Haake, *Quantum Signatures of Chaos*, 2nd ed. (Springer, New York, 2001).
[12] H.-P. Breuer and F. Petruccione, *The Theory of Open Quantum Systems* (Oxford University, Oxford, 2002).
[13] U. Weiss, *Quantum Dissipative Systems*, 4th ed. (World Scientific, Singapore, 2012).
[14] E. Knill and R. Laflamme, arXiv:quant-ph/9608012.
[15] P. W. Shor, in *Proceedings of the 37th Annual Symposium on the Foundations of Computer Science, 1996* (IEEE, New York, 1996), pp. 56–65.
[16] Y. R. Sanders, J. J. Wallman, and B. C. Sanders, New J. Phys. **18**, 012002 (2016).
[17] R. Kueng, D. M. Long, A. C. Doherty, and S. T. Flammia, Phys. Rev. Lett. **117**, 170502 (2016).
[18] M. Gutiérrez, L. Svec, A. Vargo, and K. R. Brown, Phys. Rev. A **87**, 030302(R) (2013).
[19] M. R. Geller and Z. Zhou, Phys. Rev. A **88**, 012314 (2013).
[20] D. Puzzuoli, C. Granade, H. Haas, B. Criger, E. Magesan, and D. G. Cory, Phys. Rev. A **89**, 022306 (2014).
[21] W. M. Witzel, K. Young, and S. Das Sarma, Phys. Rev. B **90**, 115431 (2014).
[22] A. S. Darmawan and D. Poulin, arXiv:1607.06460.
[23] M. Gutiérrez, C. Smith, L. Lulushi, S. Janardan, and K. R. Brown, Phys. Rev. A **94**, 042338 (2016).
[24] D. Gottesman, in *Proceedings of the XXII International Colloquium on Group Theoretical Methods in Physics*, edited by S. P. Corney, R. Delbourgo, and P. D. Jarvis (International Press, Cambridge, MA, 1999), pp. 32–43.
[25] S. Aaronson and D. Gottesman, Phys. Rev. A **70**, 052328 (2004).
[26] B. Rahn, A. C. Doherty, and H. Mabuchi, Phys. Rev. A **66**, 032304 (2002).
[27] H. Bombin and M. A. Martin-Delgado, Phys. Rev. A **76**, 012305 (2007).
[28] C. Horsman, A. G. Fowler, S. Devitt, and R. V. Meter, New J. Phys. **14**, 123011 (2012).
[29] A. Kitaev, Ann. Phys. **303**, 2 (2003).
[30] A. Cross, D. P. DiVincenzo, and B. M. Terhal, Quantum Inf. Comput. **9**, 0541 (2009).
[31] C. Cohen-Tannoudji, J. Dupont-Roc, and G. Grynberg, *Photons and Atoms* (Wiley, New York, 1989).
[32] W. Heitler, *The Quantum Theory of Radiation*, 3rd ed. (Dover, New York, 1954).
[33] R. Ernst, G. Bodenhausen, and A. Wokaun, *Principles of Nuclear Magnetic Resonance in One and Two Dimensions* (Oxford University, Oxford, 1987).
[34] A. Yariv, *Optical Electronics in Modern Communications*, 5th ed. (Oxford University, Oxford, 1996).
[35] L. Mandel and E. Wolf, *Optical Coherence and Quantum Optics* (Cambridge University, Cambridge, England, 1995).
[36] J. P. Barnes and W. S. Warren, Phys. Rev. A **60**, 4363 (1999).
[37] J. T. Merrill and K. R. Brown, Progress in compensating pulse sequences for quantum computation, in *Quantum Information and Computation for Chemistry*, edited by Sabre Kais, Advances in Chemical Physics Vol. 154 (Wiley & Sons, New York, 2014), pp. 241–294.
[38] D. P. DiVincenzo and P. Aliferis, Phys. Rev. Lett. **98**, 020501 (2007).
[39] K. M. Svore, A. W. Cross, I. L. Chuang, and A. V. Aho, Quantum Inf. Comput. **6**, 193 (2006).
[40] Y. Tomita and K. M. Svore, Phys. Rev. A **90**, 062320 (2014).
[41] A. G. Fowler, A. C. Whiteside, and L. C. L. Hollenberg, Phys. Rev. Lett. **108**, 180501 (2012).
[42] J. Edmonds, Canad. J. Math. **17**, 449 (1965).
[43] J. Edmonds, J. Res. Natl. Bur. Stand. **69B**, 125 (1965).
[44] J. J. Wallman and J. Emerson, Phys. Rev. A **94**, 052325 (2016).